

Implementing a quantum cloning machine in separate cavities via the optical coherent pulse as a quantum communication bus

Meng-Zheng Zhu^{1,2} and Liu Ye^{1,*}¹*School of Physics & Material Science, Anhui University, Hefei 230039, China*²*School of Physics & Electronic Information, Huaibei Normal University, Huaibei 235000, China*

(Received 7 December 2014; published 14 April 2015)

An efficient scheme is proposed to implement a quantum cloning machine in separate cavities based on a hybrid interaction between electron-spin systems placed in the cavities and an optical coherent pulse. The coefficient of the output state for the present cloning machine is just the direct product of two trigonometric functions, which ensures that different types of quantum cloning machine can be achieved readily in the same framework by appropriately adjusting the rotated angles. The present scheme can implement optimal one-to-two symmetric (asymmetric) universal quantum cloning, optimal symmetric (asymmetric) phase-covariant cloning, optimal symmetric (asymmetric) real-state cloning, optimal one-to-three symmetric economical real-state cloning, and optimal symmetric cloning of qubits given by an arbitrary axisymmetric distribution. In addition, photon loss of the qubus beams during the transmission and decoherence effects caused by such a photon loss are investigated.

DOI: [10.1103/PhysRevA.91.042319](https://doi.org/10.1103/PhysRevA.91.042319)

PACS number(s): 03.67.Dd, 03.67.Lx

I. INTRODUCTION

Quantum key distribution (QKD) is one of the well-known topics of quantum information [1] due to the practical application in quantum communication. The basic principles of quantum mechanics protect the quantum information from exposure to unauthorized persons. As mentioned in the no-cloning theorem [2], perfect quantum cloning of an arbitrary unknown quantum state is forbidden because of the inherent property of quantum mechanics. However, with the rapid development of quantum information theory the unknown quantum state can be copied approximately with certain fidelity [3]. It is one of the reasons for the investigation of approximate quantum cloning that provide insight into the fundamental limits on the manipulation and distribution of quantum information. The other more practical reason is that these clones can be used as very efficient eavesdropping attacks on quantum key distribution protocols [4,5]. In addition, much effort [6–14] has been devoted to the realization of the optimal approximations to quantum cloning machines (QCMs) since the seminal scheme of a universal quantum cloning machine (UQCM) was presented by Bužek and Hillery [3] in 1996. Recently, some experiments on quantum cloning have been reported [5,15–24].

We present an efficient scheme for implementation of quantum cloning by considering a hybrid system based on optical coherent pulse and electron-spin systems placed in the cavities. The electron-spin systems may be achieved by single electrons trapped in quantum dots [25]. Bartkiewicz *et al.* [26] proposed a scheme which employed the electron-spin systems in separate cavities based on quantum dots to implement optimal mirror phase-covariant cloning in 2009. As van Loock *et al.* pointed out in Ref. [27], the qubit system should be placed in a cavity resonant with the light in order to obtain a sufficient interaction between the electron and the light; for the cavity, weak coupling is sufficient. In the present scheme, the optical coherent pulse, called a quantum communication

bus (qubus), sequentially interacts with two electron-spin systems placed in the separate cavities. However, in those schemes [28–36] with single-photon-based qubus, enormous difficulties appear due to the demanding requirements on the generation and detection of the photons. The present approach can circumvent this obstacle by using the continuous variables (CVs) mode as qubus, namely, the optical coherent pulse. The coherent pulse can disentangle by itself from the qubits after a sequence of qubit-qubus interactions. Thus it plays only the role of a catalyst. The measurement-free operation for qubus avoids measurement-induced errors in contrast to the previous schemes [28–30] and the present cloning transformation becomes deterministic without measurement-result-dependent postselection [37–39] or any feedforward operations on the qubits. Due to the deterministic and measurement-free operation, the present scheme has high efficiency with high success probability. Compared with the previous scheme [14], the coefficient of the output state for a quantum cloning machine is just the product of two trigonometric functions due to the controlled-rotation operation constructed. It becomes possible that the same framework can be used to accomplish different types of quantum cloning machine only by adjusting three rotated angles. The present scheme can implement one-to-two optimal symmetric (asymmetric) UQCM [3,40–42], optimal symmetric (asymmetric) phase-covariant cloning machine (PCCM) [7,41], optimal symmetric (asymmetric) real-state cloning machine (RSCM) [7,8], optimal one-to-three symmetric economical RSCM [43], and optimal symmetric cloning transformations of qubits given by an arbitrary axisymmetric distribution [44]. In addition, photon loss of the qubus mode during the transmission and decoherence effects caused by such a photon loss are investigated.

II. PROTOCOL FOR IMPLEMENTING QUANTUM CLONING MACHINE

The interaction between the coherent field mode and the matter qubit can generally be described by the Jaynes-Cummings interaction $\hbar g(a^\dagger \sigma_- + a \sigma_+)$ and in the dispersive

*Corresponding author: yeliu@ahu.edu.cn

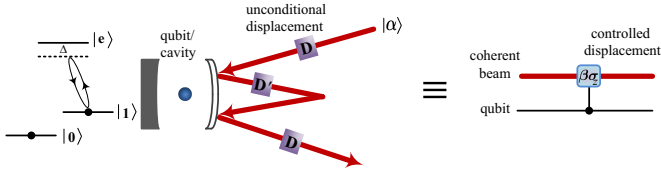


FIG. 1. (Color online) Schematic diagram of an effective controlled displacement corresponding to Eq. (2) based on unconditional displacements and conditional phase rotations. In the case of controlled displacement, $\beta \equiv 2i\alpha \sin \theta$. In the case of unconditional displacement, D and D' represent $D(\alpha \cos \theta)$ and $D(-2\alpha)$, respectively. The right figure is a simplified circuit diagram of controlled displacement.

limit (large detunings) one obtains an effective interaction Hamiltonian of the form [27,45,46]

$$H_{\text{eff}} = \hbar\chi\sigma_z a^\dagger a. \quad (1)$$

Here, a (a^\dagger) is the annihilation (creation) operator of an electromagnetic field mode in a cavity and the matter qubit is described using the conventional Pauli operators $\{\sigma_x, \sigma_y, \sigma_z\}$, with the computational basis being given by the eigenstates of $\sigma_z = |0\rangle\langle 0| - |1\rangle\langle 1|$, with $|0\rangle \equiv |\uparrow_z\rangle$ and $|1\rangle \equiv |\downarrow_z\rangle$. The matter-light coupling strength is determined via the parameter $\chi = g^2/\Delta$, where $2g$ is the vacuum Rabi splitting for the dipole transition. The optical coherent pulse is sufficiently detuned from the dipole transition, which is described by the detuning Δ , to allow a strictly dispersive light-matter interaction. The interaction H_{eff} applied for a time t generates a conditional phase rotation $\pm 2\theta$ (with $2\theta = \chi t$) on the qubit coherent state dependent upon the state of the matter qubit and the sign depends on the qubit computational basis amplitude. As shown in Fig. 1, the electron-spin system in the cavity is treated as a Ξ -configuration system, with two long-lived states $|0\rangle$ and $|1\rangle$ and an excited state $|e\rangle$. The state $|1\rangle$ can be excited to the state $|e\rangle$ via an optical coherent pulse while the transition from $|0\rangle$ to $|e\rangle$ is forbidden or extremely weak. When the optical coherent pulse interacts with the state $|1\rangle$, it picks up a small phase shift due to the $|1\rangle \leftrightarrow |e\rangle$ transition while no phase shift occurs for the state $|0\rangle$. The coherent pulse is sufficiently detuned from the transition between state $|1\rangle$ and state $|e\rangle$ to allow a strictly dispersive light-matter interaction. Local rotations between state $|0\rangle$ and state $|1\rangle$ may be achieved via stimulated Raman transitions. We may describe the effect of a conditional rotation on a coherent state and a qubit superposition state as $\exp[-i\theta a^\dagger a] \exp[-i2\theta\sigma_z a^\dagger a] (|0\rangle + |1\rangle) |\alpha\rangle = |0\rangle |\alpha e^{-i\theta}\rangle + |1\rangle |\alpha e^{i\theta}\rangle$, in which an unconditional phase operation has been imposed. The right side of the expression appears to be the effect of a single conditional rotation $\exp[-i\theta\sigma_z a^\dagger a]$ on the coherent state and the qubit superposition state with a phase shift occurring also for the state $|0\rangle$. The only requirement for a dispersive light-matter interaction resulting in a high-fidelity conditional rotation is a sufficiently large cooperativity parameter in a weak or intermediate coupling regime; the dispersive interaction does not require strong coupling [45]. Such a conditional rotation in phase space is very similar to the cross-Kerr nonlinearity for optical systems. Now it is known in the quantum optics context that such interactions can be used to implement a universal two-qubit

gate between photonic qubits based on probe coherent state measurement [47].

The centerpiece of our approach for a quantum cloning machine is a controlled displacement. In practice, it is hard to generate such a controlled displacement directly through photon-matter interactions. However, the Jaynes-Cummings-type interaction of Eq. (1) called conditional rotation is readily available. The controlled displacement relies on two operations: the conditional rotation and the unconditional displacement. In a concrete manner, this can be realized [48] with the following sequence:

$$\begin{aligned} & D(\alpha \cos \theta) \exp[-i\theta\sigma_z a^\dagger a] D(-2\alpha) \exp[i\theta\sigma_z a^\dagger a] D(\alpha \cos \theta) \\ & = D(2i\alpha \sin \theta\sigma_z), \end{aligned} \quad (2)$$

with α real. Notice that a small phase shift occurs for the state $|0\rangle$ or $|1\rangle$ using the conditional rotations in Eq. (2). Figure 1 illustrates a series of conditional rotations and unconditional displacements to simulate a controlled displacement [45,49]. The controlled displacement $D(2i\alpha \sin \theta\sigma_z)$ is exactly what we need to implement a quantum cloning machine. In the derivation of Eq. (2), we need to use the following three equations:

$$\begin{aligned} D(\beta) &= \exp(\beta a^\dagger - \beta^* a), \\ D(\beta_1)D(\beta_2) &= \exp[i\text{Im}(\beta_1\beta_2^*)]D(\beta_1+\beta_2), \\ \exp[\theta a^\dagger a] f(a, a^\dagger) \exp[-\theta a^\dagger a] &= f(ae^{-\theta}, a^\dagger e^\theta). \end{aligned} \quad (3)$$

We now demonstrate how a quantum cloning machine can be implemented via the controlled displacements from Eq. (2) and local operations on each qubit. The mechanism for the quantum cloning machine is shown in Fig. 2.

Qubit 1 of the electron-spin system in the cavity to be cloned is in the state

$$|\varphi\rangle_{a_1}^{(\text{in})} = \cos \frac{\theta}{2} |0\rangle_1 + e^{i\phi} \sin \frac{\theta}{2} |1\rangle_1, \quad (4)$$

with the polar angle $\theta \in [0, \pi]$ and the azimuthal angle $\phi \in [0, 2\pi)$ on the Bloch sphere. Qubits a_2 and a_3 are prepared respectively in the states

$$\begin{aligned} |\varphi\rangle_{a_2} &= \cos \theta_1 |0\rangle_2 + \sin \theta_1 |1\rangle_2, \\ |\varphi\rangle_{a_3} &= \cos \theta_2 |0\rangle_3 + \sin \theta_2 |1\rangle_3, \end{aligned} \quad (5)$$

through performing the suitable single-qubit rotation operation, such as a rotated angle θ_1 for the qubit a_2 in the initial state $|0\rangle_2$ and a rotated angle θ_2 for the qubit a_3 in the initial state $|0\rangle_3$.

Let us pay attention to preparing the two quantum qubits (a_2 and a_3) in a very specific state, prior to any interaction with the input qubit a_1 . The module in the dashed rectangle needs to perform two rounds in succession with the superscript $r = 1, 2$ as displayed in Fig. 2. With the help of two round operations, a controlled-rotation gate can be achieved between qubits 2 and 3. More specifically, the single-qubit operations R_{21}^1 and R_{31}^1 are performed on qubits 2 and 3 in the first round, respectively. Here $R_{21}^1 = e^{i\frac{\pi}{4}(1-\sigma_{z_2})}$, $R_{31}^1 = e^{-i\frac{\pi}{4}\sigma_{z_3}} H_3 e^{i\frac{\pi}{4}\sigma_{z_3}}$. In addition, the Hadamard operator $H_\lambda = \frac{1}{\sqrt{2}} \begin{pmatrix} 1 & 1 \\ 1 & -1 \end{pmatrix}$ with $\lambda = 1, 2, 3$. A coherent qubit mode, following four controlled-displacement interactions with two qubits a_2 and a_3 , can be used to

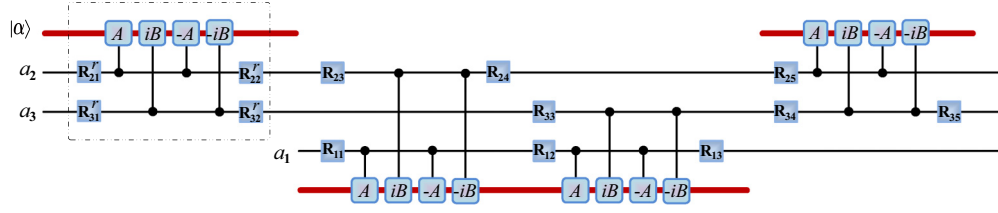


FIG. 2. (Color online) Circuit diagram of a quantum cloning machine based on controlled displacements between the optical coherent pulse and the qubits, and local operations on each qubit. In the case of controlled displacement, $A \equiv \beta_1 \sigma_z$ and $B \equiv \beta_2 \sigma_z$ with β_1, β_2 being real and $2\beta_1\beta_2 \equiv \pi/4$. The module in the dashed rectangle needs to perform two rounds in succession with the superscript $r = 1, 2$.

implement an entangling operation between the two qubits. For the case of $A \equiv \beta_1 \sigma_z$ and $B \equiv \beta_2 \sigma_z$, the sequence of controlled-displacement interactions [45,48] is defined as the total unitary operator,

$$U_{23}^{r=1} = D(-i\beta_2\sigma_{z_3})D(-\beta_1\sigma_{z_2})D(i\beta_2\sigma_{z_3})D(\beta_1\sigma_{z_2}) \\ = \exp[2i\text{Re}(\beta_1^*\beta_2)\sigma_{z_2}\sigma_{z_3}]. \quad (6)$$

Although the coherent pulse is certainly entangled with the qubits a_2 and a_3 during the controlled-displacement operations, at the end of the sequence interactions the coherent pulse is disentangled automatically from the two qubits a_2 and a_3 without requiring any subsequent measurement because the coherent qubus mode finishes in its initial state. From Eq. (6), one can observe that (1) the evolution does not depend on this coherent state; (2) the coherent pulse has effectively played the role of a catalyst. By choosing $2\beta_1\beta_2 \equiv \pi/4$, the total unitary operator as in Eq. (6) gives

$$U_{23}^{r=1} = e^{i\frac{\pi}{4}\sigma_{z_2}\sigma_{z_3}}. \quad (7)$$

After the unitary operator $U_{23}^{r=1}$ on qubits a_2 and a_3 , the single-qubit operations R_{22}^1 and R_{32}^1 are performed on qubits 2 and 3, respectively. Here, $R_{22}^1 = I$ (the symbol I denotes an identity operator) and

$$R_{32}^1 = \begin{pmatrix} \cos \frac{\theta_3}{2} & -\sin \frac{\theta_3}{2} \\ \sin \frac{\theta_3}{2} & \cos \frac{\theta_3}{2} \end{pmatrix} e^{i\frac{\pi}{4}\sigma_{z_3}} H_3.$$

Next, we perform the second round of operations on the qubits a_2 and a_3 as shown in dashed rectangle of Fig. 2. The single-qubit operations $R_{21}^2 = e^{i\frac{\pi}{4}(1-\sigma_{z_2})}$ and $R_{31}^2 = e^{-i\frac{\pi}{4}\sigma_{z_3}} H_3$ are performed on the qubits a_2 and a_3 , respectively. The sequence of controlled-displacement interactions is written as the total unitary operator $U_{23}^{r=2} = e^{i\frac{\pi}{4}\sigma_{z_2}\sigma_{z_3}}$ following the previous method. After the unitary operator $U_{23}^{r=2}$ on qubits a_2 and a_3 , the single-qubit operations R_{22}^2 and R_{32}^2 are required to perform on qubits 2 and 3, respectively. Here,

$$R_{22}^2 = \begin{pmatrix} 1 & 0 \\ 0 & i \end{pmatrix}, \\ R_{32}^2 = e^{-i\frac{\pi}{2}\sigma_{z_3}} \begin{pmatrix} \cos \frac{\theta_3}{2} & \sin \frac{\theta_3}{2} \\ -\sin \frac{\theta_3}{2} & \cos \frac{\theta_3}{2} \end{pmatrix} H_3.$$

Through the two-round operations as shown in the dashed rectangle of Fig. 2, one can simulate a controlled-rotation gate between qubits 2 and 3 with the interaction sequence as mentioned above:

$$U_{T23} = (R_{22}^2 \otimes R_{32}^2)U_{23}^{r=2}(R_{21}^2 \otimes R_{31}^2)(R_{22}^1 \otimes R_{32}^1) \\ \times U_{23}^{r=1}(R_{21}^1 \otimes R_{31}^1)$$

$$= \begin{pmatrix} 1 & 0 & 0 & 0 \\ 0 & 1 & 0 & 0 \\ 0 & 0 & \cos \theta_3 & \sin \theta_3 \\ 0 & 0 & \sin \theta_3 & -\cos \theta_3 \end{pmatrix}. \quad (8)$$

in the computational basis $\{|00\rangle_{23}, |01\rangle_{23}, |10\rangle_{23}, |11\rangle_{23}\}$. The action on the initial state $|\varphi\rangle_{a_2} \otimes |\varphi\rangle_{a_3}$ is

$$|\Phi\rangle_{23} = U_{T23}|\varphi\rangle_{a_2} \otimes |\varphi\rangle_{a_3} \\ = C_1|00\rangle_{23} + C_2|01\rangle_{23} + C_3|10\rangle_{23} + C_4|11\rangle_{23}, \quad (9)$$

where

$$C_1 = \cos \theta_1 \cos \theta_2, \\ C_2 = \cos \theta_1 \sin \theta_2, \\ C_3 = \sin \theta_1 \cos(\theta_3 - \theta_2), \\ C_4 = \sin \theta_1 \sin(\theta_3 - \theta_2). \quad (10)$$

Compared with the previous scheme [14], each coefficient (C_j with $j = 1, 2, 3, 4$) is the direct product of only two trigonometric functions due to the controlled-rotation operation constructed. This ensures that different types of quantum cloning machine can be achieved readily in the same framework by the adjustment of rotated angles.

Once the qubits (a_2 and a_3) of the quantum copier are properly prepared, then the copying of quantum information about the input state $|\varphi\rangle_{a_1}^{(in)}$ can be performed by a sequence of the following operations. In a more concrete manner, we perform the single-qubit operations $R_{11} = e^{i\frac{\pi}{4}(1-\sigma_{z_1})}$ and $R_{23} = e^{-i\frac{\pi}{4}\sigma_{z_2}} H_2$ on the qubits a_1 and a_2 , respectively. As before, four controlled-displacement interactions are expressed as a total unitary operator $U_{12} = e^{i\frac{\pi}{4}\sigma_{z_1}\sigma_{z_2}}$. After the unitary operation between qubits a_1 and a_2 , the single-qubit operation $R_{24} = H_2$ is required to perform on qubit 2. These single-qubit operations and the unitary operation are equivalent to a controlled-NOT gate between qubits a_1 and a_2 because

$$U_{T12} = (I_1 \otimes R_{24})U_{12}(R_{11} \otimes R_{23}) \\ = \begin{pmatrix} 1 & 0 & 0 & 0 \\ 0 & 1 & 0 & 0 \\ 0 & 0 & 0 & 1 \\ 0 & 0 & 1 & 0 \end{pmatrix}. \quad (11)$$

Qubits a_1 and a_2 are encoded as the control and target ones, respectively. The combined system $|\varphi\rangle_{a_1}^{(in)} \otimes |\Phi\rangle_{23}$ evolves into

$$|\Psi\rangle_{123} = U_{T12}|\varphi\rangle_{a_1}^{(in)} \otimes |\Phi\rangle_{23} \\ = \cos \frac{\theta}{2}(C_1|000\rangle + C_2|001\rangle + C_3|010\rangle + C_4|011\rangle)$$

$$\begin{aligned}
& + e^{i\phi} \sin \frac{\theta}{2} (C_1|110\rangle + C_2|111\rangle) \\
& + C_3|100\rangle + C_4|101\rangle). \tag{12}
\end{aligned}$$

Next, the single-qubit operations $R_{12} = e^{-i\frac{\pi}{4}\sigma_{z1}} H_1$ and $R_{33} = e^{i\frac{\pi}{4}(1-\sigma_{z3})}$ are performed on the qubits a_1 and a_3 , respectively. Similarly, four controlled-displacement interactions can be given by a total unitary operator $U_{13} = e^{i\frac{\pi}{4}\sigma_{z1}\sigma_{z3}}$. After the unitary operation between qubits a_1 and a_3 , the single-qubit operation R_{13} is required to perform on qubit 3, where $R_{13} = H_1$. These single-qubit operations and the unitary operation consisting of four controlled-displacement interactions are the same as the controlled-NOT gate between qubits a_1 and a_3 . At this time qubit a_1 is encoded as the target one, and qubit a_3 as the control one. In the computational basis $\{|00\rangle_{13}, |01\rangle_{13}, |10\rangle_{13}, |11\rangle_{13}\}$, three single-qubit operations and the unitary operation can be described as

$$\begin{aligned}
U_{T13} &= (R_{13} \otimes I_3)U_{13}(R_{12} \otimes R_{33}) \\
&= \begin{pmatrix} 1 & 0 & 0 & 0 \\ 0 & 0 & 0 & 1 \\ 0 & 0 & 1 & 0 \\ 0 & 1 & 0 & 0 \end{pmatrix}. \tag{13}
\end{aligned}$$

The operation in Eq. (13) evolves the system $|\Psi\rangle_{123}$ into

$$\begin{aligned}
|\Psi'\rangle_{123} &= U_{T13}|\Psi\rangle_{123} \\
&= \cos \frac{\theta}{2} (C_1|000\rangle + C_2|101\rangle + C_3|010\rangle + C_4|111\rangle) \\
&+ e^{i\phi} \sin \frac{\theta}{2} (C_1|110\rangle + C_2|011\rangle \\
&+ C_3|100\rangle + C_4|001\rangle). \tag{14}
\end{aligned}$$

Finally, in order to construct the quantum cloning machine, we will perform a controlled-NOT gate between the qubits a_2 and a_3 . More specifically, the single-qubit operations $R_{25} = e^{i\frac{\pi}{4}(1-\sigma_{z2})}$ and $R_{34} = e^{-i\frac{\pi}{4}\sigma_{z3}} H_3$ are performed on the qubits a_2 and a_3 , respectively. As mentioned above, the following four controlled-displacement interactions are represented by a total unitary operator $U_{23} = e^{i\frac{\pi}{4}\sigma_{z2}\sigma_{z3}}$. After the unitary operation between qubits a_2 and a_3 , the single-qubit operation R_{35} is required to perform on qubit 3, where $R_{35} = H_3$. All these operations can be described as

$$\begin{aligned}
U'_{T23} &= (I_2 \otimes R_{35})U_{23}(R_{25} \otimes R_{34}) \\
&= \begin{pmatrix} 1 & 0 & 0 & 0 \\ 0 & 1 & 0 & 0 \\ 0 & 0 & 0 & 1 \\ 0 & 0 & 1 & 0 \end{pmatrix}. \tag{15}
\end{aligned}$$

The quantum state $|\Psi_{\text{out}}\rangle$ is transformed into

$$\begin{aligned}
|\Psi''\rangle_{123} &= U'_{T23}|\Psi'\rangle_{123} \\
&= \cos \frac{\theta}{2} [C_1|000\rangle + (C_3|01\rangle + C_2|10\rangle)|1\rangle + C_4|110\rangle] \\
&+ e^{i\phi} \sin \frac{\theta}{2} [C_1|111\rangle + (C_3|10\rangle \\
&+ C_2|01\rangle)|0\rangle + C_4|001\rangle]. \tag{16}
\end{aligned}$$

By now we have prepared deterministically the state of Eq. (16) for quantum cloning depicted in detail in Fig. 2. For

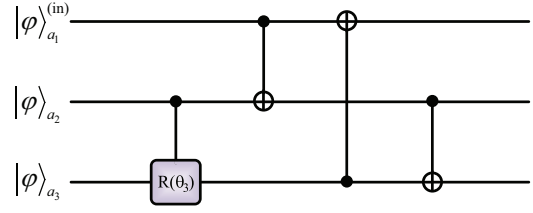


FIG. 3. (Color online) A simplified circuit of quantum cloning machine corresponding with Fig. 2. From left to right: the controlled-rotation gate and three controlled-NOT gates.

easier understanding, we simplify the quantum circuit of Fig. 2 into Fig. 3. From the left side of Fig. 3 to the right, the first component is a controlled-rotation gate described as Eq. (8) and the subsequent three components are the controlled-NOT gates in turn described as Eqs. (11), (13), and (15).

The reduced density operator of each output qubit, such as cloners a_1 and a_2 , after the cloning procedure, is given as

$$\begin{aligned}
\rho_1^{(\text{out})} &= \text{Tr}_{a_2, a_3} [|\Psi''\rangle_{123}\langle\Psi''|] = \sum_{i=1}^4 |\Psi_i\rangle_{a_1}\langle\Psi_i|, \\
\rho_2^{(\text{out})} &= \text{Tr}_{a_1, a_3} [|\Psi''\rangle_{123}\langle\Psi''|] = \sum_{i=1}^4 |\Phi_i\rangle_{a_2}\langle\Phi_i|, \tag{17}
\end{aligned}$$

with

$$\begin{aligned}
|\Psi_{k\mp 1}\rangle_{a_1} &\equiv \cos \frac{\theta}{2} C_{k\mp 1}|0\rangle_1 + e^{i\phi} \sin \frac{\theta}{2} C_{k\pm 1}|1\rangle_1, \\
|\Phi_{j+l}\rangle_{a_2} &\equiv \cos \frac{\theta}{2} C_{j+l}|0\rangle_2 + e^{i\phi} \sin \frac{\theta}{2} C_{\bar{j}+l}|1\rangle_2, \\
j &= 1, 2; k = 2, 3; l = 0, 2. \tag{18}
\end{aligned}$$

Here the value of \bar{j} is opposite to j . In the symmetric cloning process, the quantum information in the initial qubit a_1 is copied to qubits a_1 and a_2 equally well so that the reduced density matrices at the output are identical, and the fidelities used to evaluate the quality of the cloning transformation are also identical. From Eq. (17) the corresponding fidelity between the reduced density operator of each output copy and the input state is described as

$$\begin{aligned}
F_i &= {}_{a_1}^{(\text{in})}\langle\phi|\rho_i^{(\text{out})}|\phi\rangle_{a_1}^{(\text{in})} \\
&= C_1^2 + C_{3-\delta_{2,i}}^2 + \sin^2\theta [C_4^2 + C_{3-\delta_{1,i}}^2 - (C_1 - C_{3-\delta_{2,i}})^2 \\
&+ (e^{2i\phi} + e^{-2i\phi})C_{3-\delta_{1,i}}C_4]/2, \tag{19}
\end{aligned}$$

with $i = 1, 2$. Here $\delta_{j,i}$ is the Kronecker delta. So far the preliminary scheme about quantum cloning has been accomplished. Then we will discuss how to implement different types of quantum cloning machine based on the result in Eq. (16) by regulating the rotated angle θ_i with $i = 1, 2, 3$.

If the three rotated angles satisfy $\tan\theta_1 + \sin\theta_2 = \cos\theta_2$ and $\theta_3 = \theta_2$, we will implement an optimal one-to-two asymmetric UQCM (AUQCM) [40–42] where the quantum information in the original qubit a_1 , such as $\theta \in [0, \pi]$ and $\phi \in [0, 2\pi)$, is completely unknown. We describe such a copying process in which the two fidelities do not depend on the parameters θ, ϕ of the input state. That is to say, there is the same quality of cloning transformation for an arbitrary input state. A quantum cloning machine with this feature is a universal one. The condition of $\theta_3 = \theta_2$ stems from the

relation $C_4 = 0$, which makes the fidelities in Eq. (19) be phase independent. The other condition of $\tan \theta_1 + \sin \theta_2 = \cos \theta_2$ originates from the relation $C_1 = C_2 + C_3$. The relations $C_1 = C_2 + C_3$ and $C_4 = 0$ ensure that the quality of the cloning is independent of the input states. According to the specific relations given above, from Eq. (19) we can easily calculate the fidelities of two clones,

$$F_1 = (1 + p^2)/N^2, \quad F_2 = (1 + q^2)/N^2, \quad (20)$$

where $p = \tan \theta_1 / \cos \theta_2$, $q = \tan \theta_2$, and $N \equiv \sqrt{1 + p^2 + q^2} = (\cos \theta_1 \cos \theta_2)^{-1}$. In this case, the cloning transformation of the optimal AUQCM can be written as

$$\begin{aligned} & \cos \frac{\vartheta}{2} [|000\rangle + (p|01\rangle + q|10\rangle)|1\rangle] / N \\ & + e^{i\phi} \sin \frac{\vartheta}{2} [|111\rangle + (p|10\rangle + q|01\rangle)|0\rangle] / N, \end{aligned} \quad (21)$$

according to the result, Eq. (4.3), given by Ghu in [42] with the coefficients $p, q \geq 0$ satisfying $p + q = 1$. For this reason, we can redefine the coefficients p, q as functions of the optimal angle ϑ , such as $p \equiv \cos^2 \vartheta$ and $q \equiv \sin^2 \vartheta$ with $\vartheta \in [0, \pi/2]$. The requirement for the coefficients $p, q \geq 0$ and $p + q = 1$ limits the range of rotated angles θ_1 and θ_2 , so that $\theta_1 \in [0, \arctan \sqrt{(\sqrt{5} - 1)/2}]$ and $\theta_2 \in [0, \pi/4]$. If the rotated angle θ_1 is set for $\arctan(\sqrt{1/5})$ and θ_2 for $\arctan(1/2)$, we will find out there will be such a transition from optimal AUQCM to optimal symmetric UQCM (SUQCM) [3]. In this case, the fidelities $F_1 = F_2 = 5/6$ and the coefficients $p = q = 1/2$ and $N = \sqrt{3/2}$. Thus the state of the three qubits in Eq. (16) can be described as [3]

$$\begin{aligned} & \cos \frac{\vartheta}{2} \left[\sqrt{\frac{2}{3}} |000\rangle + \sqrt{\frac{1}{3}} |+\rangle |1\rangle \right] \\ & + e^{i\phi} \sin \frac{\vartheta}{2} \left[\sqrt{\frac{2}{3}} |111\rangle + \sqrt{\frac{1}{3}} |+\rangle |0\rangle \right], \end{aligned} \quad (22)$$

where $|+\rangle \equiv (|01\rangle + |10\rangle)/\sqrt{2}$.

AUQCM or SUQCM produces two copies with the invariable quality for all possible input states. However, if partial prior knowledge of the input state to be cloned is available, or it is known to belong to a subset of all possible input states, then it is probable to clone the state with a higher fidelity. Take the states whose Bloch vector lies in the equator of the Bloch sphere—for example, the so-called phase covariant, used for the first time by Bruß, *et al.* [7], is derived from the fact that the fidelity of cloning will not depend on the azimuthal angle ϕ . For the present scheme, if the joint relations of the three rotated angles meet the conditions of $\cos \theta_1 \cos \theta_2 = 1/\sqrt{2}$ and $\theta_3 = \theta_2$, we will implement an optimal one-to-two asymmetric PCCM (APCCM) [41] where the prior knowledge of the original input state is the polar angle (fixed to $\pi/2$) of a vector on the Bloch sphere with the azimuthal angle completely unknown $\phi \in [0, 2\pi)$. For the optimal APCCM, the state of the three qubits in Eq. (16) can be written as [41]

$$\begin{aligned} & \{ [|000\rangle + (\cos \vartheta |01\rangle + \sin \vartheta |10\rangle)|1\rangle] / \sqrt{2} \\ & + e^{i\phi} [|111\rangle + (\cos \vartheta |10\rangle + \sin \vartheta |01\rangle)|0\rangle] / \sqrt{2} \} / \sqrt{2}, \end{aligned} \quad (23)$$

where $\sin \vartheta = \sqrt{2 \cos^2 \theta_1 - 1}$ and $\cos \vartheta = \sqrt{2} \sin \theta_1$ with $\vartheta \in [0, \pi/2]$. Then we can easily calculate the fidelities of two clones,

$$F_1 = (1 + \cos \vartheta)/2, \quad F_2 = (1 + \sin \vartheta)/2. \quad (24)$$

This ($\vartheta \in [0, \pi/2]$) limits the rotated angles within the range $\theta_1, \theta_2 \in [0, \pi/4]$. If the specific values are assigned to the angles θ_1 and θ_2 , such as $\theta_1 \equiv \pi/6$ and $\theta_2 \equiv \arcsin(1/\sqrt{3})$, the APCCM will reduce to an optimal one-to-two symmetric PCCM (SPCCM) [7]. Under this condition, the fidelities $F_1 = F_2 = \frac{1}{2}(1 + \frac{1}{\sqrt{2}})$ and the coefficients $\cos \vartheta = \sin \vartheta = 1/\sqrt{2}$. Thus the state of three qubits in Eq. (16) can be described as [7]

$$\frac{1}{\sqrt{2}} \left[\frac{1}{\sqrt{2}} (|000\rangle + |+\rangle |1\rangle) + e^{i\phi} \frac{1}{\sqrt{2}} (|111\rangle + |+\rangle |0\rangle) \right]. \quad (25)$$

Because the equatorial states with $\phi = 0, \pi/2, \pi, 3\pi/2$ are used as the encoded states in the BB84 cryptographic scheme [50], proposed by Bennett and Brassard in 1984, for its significant uses in the well-known QKD protocol [1,51], copying the equatorial states has obtained extensive attention.

The comparison between fidelities of APCCM with those of AUQCM is plotted in Fig. 4. From the viewpoint of optimal angle ϑ , the fidelity of clone a_1 or a_2 in APCCM is not permanently greater than the corresponding one in AUQCM. As functions of the rotated angle θ_1 , the fidelity of qubit a_2 in APCCM is distinctly better than that in AUQCM, but the cloning fidelity of qubit a_1 in APCCM is slightly worse than that in AUQCM. The difference between the sum of the fidelities a_1, a_2 for APCCM and one for AUQCM as a function of ϑ and θ_1 is shown in Figs. 4(c) and 4(d), respectively. In the perspective of total fidelity as a function of θ_1 , it is in accord with the rule that the restriction of the input state to the equator of the Bloch sphere improves the cloning performance.

We consider the input state to be cloned at the equator in the x - z plane instead of the x - y equator. This requires *a priori* known value of the azimuthal angle ϕ for the initial input

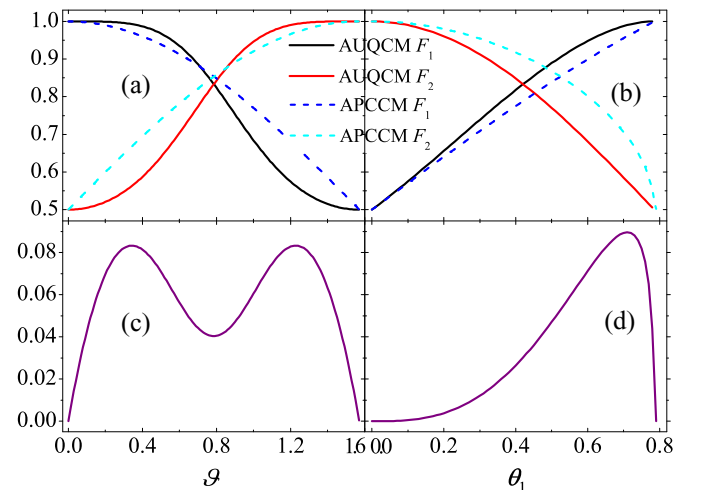


FIG. 4. (Color online) The fidelities of AUQCM and APCCM as functions of (a) the optimal angle ϑ , (b) the rotated angle θ_1 ; the difference between the sum of the fidelities a_1, a_2 for APCCM and one for AUQCM versus (c) ϑ , (d) θ_1 .

state, such as 0 or π . Thus the initial state can be described as $|\varphi\rangle_{a_1}^{(\text{in})} = \cos\frac{\theta}{2}|0\rangle_1 + \sin\frac{\theta}{2}|1\rangle_1$ with $\theta \in [0, \pi] \cup [-\pi, 0]$ due to $\phi = 0$ or π in the real states. This type of restrictive quantum cloning is referred to as the real-state cloning machine [8]. From the viewpoint of the rotated spherical coordinate, e.g., the vector $|\psi\rangle = \cos\frac{\theta_0}{2}|0\rangle + e^{i\phi_0}\sin\frac{\theta_0}{2}|1\rangle$ with $\theta_0 = \phi_0 = \pi/2$ as the new polar axis of the Bloch sphere [44], RSCM is just a conventional PCCM in essence. The optimization of asymmetric RSCM (ARSCM) becomes very simple in the way which is proposed by Bartkiewicz *et al.* [44] to tackle the symmetric cloning for an arbitrary axisymmetric distribution of qubits, avoiding the complicated deduction in [8]. According to the change of basis, the unitary transformation matrix

$$S = \begin{pmatrix} \cos\frac{\theta_0}{2} & e^{-i\phi_0}\sin\frac{\theta_0}{2} \\ e^{i\phi_0}\sin\frac{\theta_0}{2} & -\cos\frac{\theta_0}{2} \end{pmatrix} \quad (26)$$

connects the old orthonormal set $\{|0\rangle, |1\rangle\}$ and the new orthonormal set $\{|\psi\rangle, |\bar{\psi}\rangle\}$, where $|\bar{\psi}\rangle$ is a state orthogonal to $|\psi\rangle$. Using the change of the representation we can transform an expression of RSCM in the old orthonormal basis,

$$\begin{aligned} & \cos\frac{\theta}{2}[C_1|000\rangle + (C_3|01\rangle + C_2|10\rangle)|1\rangle + C_4|110\rangle] \\ & + \sin\frac{\theta}{2}[C_1|111\rangle + (C_3|10\rangle + C_2|01\rangle)|0\rangle + C_4|001\rangle], \end{aligned} \quad (27)$$

into one in the new orthonormal basis,

$$\begin{aligned} & ie^{-i\frac{\theta}{2}} \left\{ \frac{1}{\sqrt{2}}[C'_1|\bar{\psi}\bar{\psi}\bar{\psi}\rangle + (C'_3|\bar{\psi}\psi\rangle + C'_2|\psi\bar{\psi}\rangle)|\psi\rangle \right. \\ & + C'_4|\psi\psi\bar{\psi}\rangle] + \frac{1}{\sqrt{2}}e^{i(\theta+\frac{\pi}{2})}[C'_1|\psi\psi\psi\rangle + (C'_3|\psi\psi\bar{\psi}\rangle \\ & \left. + C'_2|\bar{\psi}\psi\rangle)|\bar{\psi}\rangle + C'_4|\bar{\psi}\bar{\psi}\psi\rangle] \right\}, \end{aligned} \quad (28)$$

where $C'_j \equiv [\sum_{k=1}^4 (-1)^{\delta_{j,k}} C_k]/2$ with $j = 1, 2, 3, 4$. The initial input state becomes $|\varphi\rangle_{a_1}^{(\text{in})} = e^{-i\frac{\theta}{2}}[\frac{1}{\sqrt{2}}|\psi\rangle + \frac{1}{\sqrt{2}}e^{i(\theta+\frac{\pi}{2})}|\bar{\psi}\rangle]$ in the new computational basis. We can ignore the global phases $ie^{-i\theta/2}$ and $e^{-i\theta/2}$ at the beginning because they have no observable effects. This is commonly known as phase-covariant cloning from the form of initial input state in the new orthonormal basis. The fidelities of the transformation in Eq. (28) for the clones can be described as

$$\begin{aligned} F'_j &= \frac{1}{2} \left[2C'_4C'_{2+\delta_{2,j}} + C'_{3-\delta_{2,j}}C'_1(e^{-2i\gamma'} + e^{2i\gamma'}) \right. \\ & \left. + \sum_{i=1}^4 C'_i{}^2 \right], \end{aligned} \quad (29)$$

with $j = 1, 2$. Obviously, the condition $C'_1 = 0$ means that the cloning transformation is phase independent. We can further obtain the expressions of C'_2, C'_3, C'_4 by optimizing the fidelity, e.g., $C'_2 = \frac{1}{\sqrt{2}}\cos\vartheta$, $C'_3 = \frac{1}{\sqrt{2}}\sin\vartheta$, and $C'_4 = \frac{1}{\sqrt{2}}$. Therefore, the coefficients in Eq. (27) for the optimal ARSCM are

$$C_j = [(-1)^{\delta_{4,j}} + (-1)^{\delta_{2,j}}\cos\vartheta + (-1)^{\delta_{3,j}}\sin\vartheta]/\sqrt{8}, \quad (30)$$

with $j = 1, 2, 3, 4$. And from Eq. (19) the fidelities are $F_1 = (1 + \cos\vartheta)/2$, $F_2 = (1 + \sin\vartheta)/2$ with the optimal angle $\vartheta \in [0, \pi/2]$. The relation expression $C_1 - C_4 = C_2 + C_3$, due to $C'_1 = 0$, ensures that the fidelities are independent of the equatorial input states in the $x-z$ plane. If the relationship between optimal angle ϑ and rotated angles $\theta_1, \theta_2, \theta_3$ satisfies $\cos\vartheta = \sqrt{2}\cos\theta_1(\cos\theta_2 - \sin\theta_2) = 2\cos\theta_1(\cos\theta_1 - \sqrt{2}\sin\theta_2)$, $\sin\vartheta = \cos 2\theta_1 = 1 + \sqrt{2}\sin\theta_1[\sin(\theta_3 - \theta_2) - \cos(\theta_3 - \theta_2)]$ in the present scheme, we can implement an optimal ARSCM. The range of rotated angles is $\theta_1, \theta_2, \theta_3 - \theta_2 \in [0, \pi/4]$ due to the restrictive condition of optimal angle $\vartheta \in [0, \pi/2]$. When we assign the specific values to the rotated angles θ_1, θ_2 , and θ_3 , such as $\theta_1 = \theta_2 = \pi/8$ and $\theta_3 = \pi/4$, the present scheme will implement an optimal one-to-two symmetric RSCM (SRSCM) [8], which is also referred to as the optimal SPCCM in [7]. Under the constraint of the given angles $\theta_1, \theta_2, \theta_3$, the parameters $\cos\vartheta = \sin\vartheta = 1/\sqrt{2}$ and the fidelities $F_1 = F_2 = \frac{1}{2}(1 + \frac{1}{\sqrt{2}})$. The optimal SPCCM transformation can be described explicitly as follows [7]:

$$\begin{aligned} & \cos\frac{\theta}{2} \left[\left(\frac{1}{2} + \frac{1}{\sqrt{8}} \right) |000\rangle + \frac{1}{2} |+\rangle|1\rangle + \left(\frac{1}{2} - \frac{1}{\sqrt{8}} \right) |110\rangle \right] \\ & + \sin\frac{\theta}{2} \left[\left(\frac{1}{2} + \frac{1}{\sqrt{8}} \right) |111\rangle + \frac{1}{2} |+\rangle|0\rangle \right. \\ & \left. + \left(\frac{1}{2} - \frac{1}{\sqrt{8}} \right) |001\rangle \right]. \end{aligned} \quad (31)$$

The present scheme can implement an optimal one-to-three symmetric economical RSCM (SERSCM) proposed by Fan *et al.* [43]. With *a priori* knowledge of the azimuthal angle (i.e., $\phi = 0$ or π) and the polar angle being completely unknown, the optimal SERSCM can be determined as follows [43]:

$$\begin{aligned} & \cos\frac{\theta}{2} \left[\frac{\sqrt{3}}{2} |000\rangle + \frac{1}{\sqrt{12}}(|011\rangle + |101\rangle + |110\rangle) \right] \\ & + \sin\frac{\theta}{2} \left[\frac{\sqrt{3}}{2} |111\rangle + \frac{1}{\sqrt{12}}(|100\rangle + |010\rangle + |001\rangle) \right], \end{aligned} \quad (32)$$

with $\theta \in [0, \pi] \cup [-\pi, 0]$. For each of three clones, the fidelity is $F = 5/6$. To implement the optimal SERSCM, the rotated angles of the present scheme can be chosen as $\theta_1 = \arcsin\sqrt{1/6}$, $\theta_2 = \arcsin\sqrt{1/10}$, and $\theta_3 = \pi/4 + \arcsin\sqrt{1/10}$.

As mentioned above, the cloning transformations in our scheme are based on the special axisymmetric distribution on the Bloch sphere for the qubits to be cloned, e.g., along the vector $(|0\rangle + i|1\rangle)/\sqrt{2}$ for the RSCM and along the vector $|0\rangle$ for the rest cloning. The present scheme can also implement a cloning transformation of an arbitrary axisymmetric distribution [44] with the highest fidelity. Suppose we know the pure state $|\psi\rangle = \cos\frac{\theta_0}{2}|0\rangle + e^{i\phi_0}\sin\frac{\theta_0}{2}|1\rangle$, which acts as the polar axis of the rotated spherical coordinate; in the new spherical coordinate we can express all other qubit states on the Bloch sphere as

$$|\psi(\theta', \phi')\rangle = \cos\frac{\theta'}{2}|\psi\rangle + e^{i\phi'}\sin\frac{\theta'}{2}|\bar{\psi}\rangle. \quad (33)$$

The symbol θ' is a polar angle and ϕ' is an azimuth angle in the new coordinate corresponding to the Bloch vector $|\psi\rangle$ as the polar axis. The one-to-two symmetric cloning transformation for an arbitrary distribution of qubits in Eq. (33) can be expressed as

$$\begin{aligned} & \cos \frac{\theta'}{2} [\cos \alpha_+ (\cos \beta_+ |\psi\rangle\langle\psi|) \\ & + \sin \beta_+ |\bar{\psi}\bar{\psi}\rangle_{12} |\bar{\psi}\rangle_3 + \sin \alpha_+ |\psi_+\rangle_{12} |\psi\rangle_3] \\ & + e^{i\phi'} \sin \frac{\theta'}{2} [\cos \alpha_- (\cos \beta_- |\bar{\psi}\bar{\psi}\rangle + \sin \beta_- |\psi\psi\rangle)_{12} |\psi\rangle_3 \\ & + \sin \alpha_- |\psi_+\rangle_{12} |\bar{\psi}\rangle_3], \end{aligned} \quad (34)$$

where $|\psi_+\rangle = (|\psi\bar{\psi}\rangle + |\bar{\psi}\psi\rangle)/\sqrt{2}$. For the sake of simplicity, Ref. [44] mainly paid attention to axisymmetric distributions. The axisymmetric distribution for qubits to be cloned means that the cloning transformation is phase independent. Under the condition of $|\Gamma| > 1$, which is a parameter in [44], and $\alpha_{\pm} = \alpha$ and $\beta_{\pm} = 0$, the fidelity of the symmetric cloning for an arbitrary axisymmetric distribution of qubits can be described as

$$F = F_1 = F_2 = \eta_0 P_0(\cos \theta') + \eta_2 P_2(\cos \theta'), \quad (35)$$

with $\eta_0 = \frac{1}{2}(1 + \cos^2 \alpha) - \eta_2$, $\eta_2 = -\frac{1}{3}(\frac{\sin 2\alpha}{\sqrt{2}} - \cos^2 \alpha)$. Here $P_n(\cos \theta')$ is the Legendre polynomial. If $\alpha \equiv \arctan(1/\sqrt{2})$ corresponds to the coefficient $\eta_2 = 0$, the transformation represents the SUQCM [3] for an arbitrary axisymmetric distribution with the fidelity $F = 5/6$. If $\cos \alpha \equiv \sqrt{1 + \cos^2 \theta'}/\sqrt{P}/\sqrt{2}$ with $P = 2 - 4\cos^2 \theta' + 3\cos^4 \theta'$, the transformation denotes an optimal mirror phase-covariant cloning (MPCC) [26]. Especially for θ' fixed to $\pi/2$, the optimal MPCC machine reduces to the optimal SPCCM [7,52] in the new computational basis. Our scheme can implement these symmetric cloning transformations for an arbitrary axisymmetric distribution using the approach which is analogous to the one for optimizing the ARSCM above. Because the change of representation can transform Eq. (16) in the old orthonormal basis $\{|0\rangle, |1\rangle\}$ into an expression in the new orthonormal basis $\{|\psi\rangle, |\bar{\psi}\rangle\}$, we can express the coefficient C_j ($j = 1, 2, 3, 4$) in Eq. (16) as a function of the parameter α through comparing the expression with Eq. (34) in the case of $\alpha_{\pm} = \alpha$ and $\beta_{\pm} = 0$. That is to say, the relation between the rotated angle θ_l ($l = 1, 2, 3$) and the parameter α can be established based on the change of basis.

III. EFFECT DUE TO THE QUBUS PHOTON LOSSES

For clarity, we have discussed above the implementation of quantum cloning machines in the absence of the qubus photon loss. In what follows, we shall investigate the decoherence effect of photon losses of the qubus pulse through utilizing the approach provided in [53–56]. To implement the controlled displacement in Eq. (2), it seems to be necessary to couple the qubus coherent pulse out of the cavity and back into it every time when an unconditional displacement must be applied through an external local oscillator field. However, this rather inefficient feature can be avoided in an all-cavity-based approach. This approach is to perform the unconditional displacement through driving the qubus pulse directly with

an intense classical pump. It is no longer needed to couple the optical pulses out of the cavities for performing the unconditional displacement so as to reduce the degrading effect of photon losses [48]. In spite of this, the qubus pulse is still required in and out of two cavities in order to accomplish an interaction with both qubits placed in different cavities. Take such a stage; for an example, we investigate the decoherence effect of qubus photon losses. After the qubus coherent pulse in the state $|2\alpha\rangle_C$ interacts with qubit a_2 as described by Eq. (2), it is sent to a neighboring cavity and is just preparing to interact with the other qubit a_3 . Ideally, the stage without the photon losses of qubus pulse can be described as

$$|\psi(\beta)\rangle_{a_2C}^{(id)} = \cos \theta_1 |0\rangle_2 |\beta e^{i\phi}\rangle_C + \sin \theta_1 |1\rangle_2 |\beta e^{-i\phi}\rangle_C, \quad (36)$$

where $\beta \equiv 2\alpha\sqrt{1 + \sin^2 \theta}$, $e^{\pm i\phi} \equiv (1 \pm i \sin \theta)/\sqrt{1 + \sin^2 \theta}$. Photon losses in the qubus channel can be modeled by considering a simple beam splitter, which reflects, on average, $1 - \eta$ photons into an environment mode. For simplicity, the environment mode is assumed initially in the vacuum state [57]. Therefore, this stage can be rewritten as

$$\begin{aligned} |\psi\rangle_{a_2CE} &= \cos \theta_1 |0\rangle_2 |\sqrt{\eta}\beta e^{i\phi}\rangle_C |\sqrt{1-\eta}\beta e^{i\phi}\rangle_E \\ &+ \sin \theta_1 |1\rangle_2 |\sqrt{\eta}\beta e^{-i\phi}\rangle_C |\sqrt{1-\eta}\beta e^{-i\phi}\rangle_E. \end{aligned} \quad (37)$$

We may now define a set of orthogonal, two-dimensional basis $\{|u\rangle, |v\rangle\}$ for the environment mode [58]:

$$\begin{aligned} |\sqrt{1-\eta}\beta e^{i\phi}\rangle_E &\equiv (\mu_E |u\rangle_E + \nu_E |v\rangle_E) e^{i(1-\eta)\xi}, \\ |\sqrt{1-\eta}\beta e^{-i\phi}\rangle_E &\equiv (\mu_E |u\rangle_E - \nu_E |v\rangle_E) e^{-i(1-\eta)\xi}, \end{aligned} \quad (38)$$

with

$$\begin{aligned} \nu_E &= \sqrt{1 - \mu_E^2}; \quad \mu_E = [1 + e^{-8(1-\eta)\alpha^2 \sin^2 \theta}]^{1/2} / \sqrt{2}, \\ \xi &= 4\alpha^2 \sin \theta. \end{aligned} \quad (39)$$

The reduced density matrix for tracing over the loss mode can be expressed as

$$\begin{aligned} \rho_{a_2C} &= \text{Tr}_E[|\psi\rangle_{a_2CE}\langle\psi|] \\ &= \cos^2 \theta_1 |0\rangle_2 \langle 0| |\sqrt{\eta}\beta e^{i\phi}\rangle_C \langle \sqrt{\eta}\beta e^{i\phi}| + e^{2i(1-\eta)\xi} (2\mu_E^2 - 1) \\ &\quad \times \cos \theta_1 \sin \theta_1 |0\rangle_2 \langle 1| |\sqrt{\eta}\beta e^{i\phi}\rangle_C \langle \sqrt{\eta}\beta e^{-i\phi}| \\ &\quad + e^{-2i(1-\eta)\xi} (2\mu_E^2 - 1) \cos \theta_1 \sin \theta_1 |1\rangle_2 \langle 0| |\sqrt{\eta}\beta e^{-i\phi}\rangle_C \\ &\quad \times \langle \sqrt{\eta}\beta e^{i\phi}| + \sin^2 \theta_1 |1\rangle_2 \langle 1| |\sqrt{\eta}\beta e^{-i\phi}\rangle_C \langle \sqrt{\eta}\beta e^{-i\phi}|. \end{aligned} \quad (40)$$

The decoherence in the photon loss leads to a damping factor determined by ξ and $-2(1-\eta)(2\alpha \sin \theta)^2$. We can find that the entangled state about the qubus mode and qubit a_2 is subject to decoherence and becomes mixed due to the presence of photon loss. This decohered state obviously will have less entanglement than that in Eq. (36). A relevant measure of how much useful entanglement remained is the overlap of

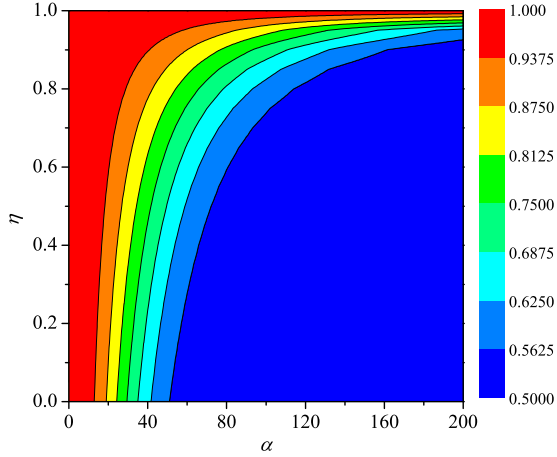


FIG. 5. (Color online) The fidelity as a function of α, η for the phase $\theta = 0.01$, $\alpha \in [0, 200]$ and $\eta \in [0, 1]$.

ρ_{a_2C} with states of the form (36). However, as Enk and Hirota mentioned in [57], the maximum overlap is in fact with the state $|\psi(\sqrt{\eta}\beta)\rangle_{a_2C}^{(id)}$. The fidelity is defined as the maximum overlap,

$$F = \frac{(\text{id})}{a_2C} \langle \psi(\sqrt{\eta}\beta) | \rho_{a_2C} | \psi(\sqrt{\eta}\beta) \rangle_{a_2C}^{(\text{id})} = \{1 + \exp[-8(1 - \eta)\alpha^2 \sin^2 \theta]\} / 2. \quad (41)$$

We can easily observe from Fig. 5 that the fidelity decreases with decreasing the transmission parameter η while it increases with decreasing α . A reasonable length for the individual cavities of the quantum cloning machine would be 1 m so that the transmission parameter η approaches unit. The reduced density matrix in Eq. (40) approaches the pure state $|\psi(\sqrt{\eta}\beta)\rangle_{a_2C}^{(id)}$ for small α . However, this pure state is nearly unentangled for too small α . In other words, it is almost a product state of the single-photon a_2 and the basis vector $|u\rangle_C$ corresponding to one component of the expanded qubus mode in Eq. (36) with the orthogonal, two-dimensional basis $\{|u\rangle, |v\rangle\}$. In addition, due to photon loss the controlled displacement on the qubus mode is no longer exactly the one desired, leading to a smaller phase shift and an error in the gate, to such an extent that the qubus mode will not disentangle exactly from the qubits. As long as the degree of loss is known, these effects can be eliminated by increasing the amplitude of the controlled displacement [48].

IV. CONCLUSION

We present a scheme for deterministic implementation of quantum cloning by using an optical coherent pulse as qubus to mediate interaction between the electron-spin systems placed in the separate cavities, instead of direct qubit-qubit interaction. The distinct advantage of our scheme is that (1) the quantum information is encoded into discrete variables (DVs), namely, the electron-spin system in the individual cavity while the CVs mode, the optical coherent pulse, plays the role of a quantum communication bus to mediate interactions. In those schemes [28–36] with single-photon-based qubus, enormous difficulties arise due to the requirements on the generation and detection of the photons. As is known to all, the performance of a successful near-deterministic gate is indispensable from efficient detectors which unambiguously detect a single photon. The present approach to circumvent this obstacle is based on the CVs mode. (2) The entangled qubit pair (two electron-spin systems in separate cavities) is constructed deterministically through a sequence of qubit-qubus interactions without requiring any subsequent measurement because the qubus mode is disentangled automatically from the qubits at the end of the interactions. Thus the present cloning scheme could effectively avoid measurement-induced errors. Additionally, the measurement-free operation in the present scheme not only simplifies the cloning procedure, but also makes the cloning transformation faster. Due to the deterministic and measurement-free operation in our scheme, the success probability of quantum cloning, which is unit in principle, is superior to the previously reported ones [37–39]. (3) In contrast to the previous scheme [14], the coefficient of the output state of our cloning machine is just the product of two trigonometric functions due to introducing the controlled-rotation operation. This ensures that different types of quantum cloning machine could be achieved readily in the same framework by appropriately adjusting the rotated angles. The present scheme can implement optimal one-to-two symmetric (asymmetric) UQCM, optimal symmetric (asymmetric) PCCM, optimal symmetric (asymmetric) RSCM, optimal one-to-three symmetric economical RSCM, and optimal symmetric cloning of qubits given by an arbitrary axisymmetric distribution.

ACKNOWLEDGMENTS

This work was supported by the National Natural Science Foundation of China under Grants No. 11074002 and No. 61275119, and also the Doctoral Fund of Ministry of Education of China under Grant No. 20103401110003.

[1] V. Scarani, H. Bechmann-Pasquinucci, N. J. Cerf, M. Dušek, N. Lütkenhaus, and M. Peev, *Rev. Mod. Phys.* **81**, 1301 (2009).
 [2] W. K. Wootters and W. H. Zurek, *Nature* **299**, 802 (1982).
 [3] V. Bužek and M. Hillery, *Phys. Rev. A* **54**, 1844 (1996).
 [4] J. Fiurášek and N. J. Cerf, *Phys. Rev. A* **77**, 052308 (2008).
 [5] K. Bartkiewicz, K. Lemr, A. Cernoch, J. Soubusta, and A. Miranowicz, *Phys. Rev. Lett.* **110**, 173601 (2013).

[6] H. Fan, K. Matsumoto, X. B. Wang, and H. Imai, *J. Phys. A: Math. Gen.* **35**, 7415 (2002).
 [7] D. Bruß, M. Cinchetti, G. M. D’Ariano, and C. Macchiavello, *Phys. Rev. A* **62**, 012302 (2000).
 [8] W. H. Zhang, T. Wu, L. Ye, and J. L. Dai, *Phys. Rev. A* **75**, 044303 (2007).
 [9] L. M. Duan and G. C. Guo, *Phys. Rev. Lett.* **80**, 4999 (1998).

- [10] V. Scarani, S. Iblisdir, N. Gisin, and A. Acín, *Rev. Mod. Phys.* **77**, 1225 (2005).
- [11] W. H. Zhang and L. Ye, *New J. Phys.* **9**, 318 (2007).
- [12] W. H. Zhang, L. B. Yu, and L. Ye, *Phys. Lett. A* **356**, 195 (2006).
- [13] W. H. Zhang, L. B. Yu, L. Ye, and J. L. Dai, *Phys. Lett. A* **360**, 726 (2007).
- [14] V. Bužek, S. L. Braunstein, M. Hillery, and D. Bruß, *Phys. Rev. A* **56**, 3446 (1997).
- [15] A. Lamas-Linares, C. Simon, J. C. Howell, and D. Bouwmeester, *Science* **296**, 712 (2002).
- [16] A. Cernoch, L. Bartušková, J. Soubusta, M. Ježek, J. Fiurášek, and M. Dušek, *Phys. Rev. A* **74**, 042327 (2006).
- [17] J. Soubusta, L. Bartušková, A. Cernoch, J. Fiurášek, and M. Dušek, *Phys. Rev. A* **76**, 042318 (2007).
- [18] E. Nagali, T. De Angelis, F. Sciarrino, and F. De Martini, *Phys. Rev. A* **76**, 042126 (2007).
- [19] M. Sabuncu, U. L. Andersen, and G. Leuchs, *Phys. Rev. Lett.* **98**, 170503 (2007).
- [20] H. K. Cummins, C. Jones, A. Furze, N. F. Soffe, M. Mosca, J. M. Peach, and J. A. Jones, *Phys. Rev. Lett.* **88**, 187901 (2002).
- [21] J. Du, T. Durt, P. Zou, H. Li, L. C. Kwek, C. H. Lai, C. H. Oh, and A. Ekert, *Phys. Rev. Lett.* **94**, 040505 (2005).
- [22] H. W. Chen, X. Y. Zhou, D. Suter, and J. F. Du, *Phys. Rev. A* **75**, 012317 (2007).
- [23] K. Bartkiewicz, A. Cernoch, K. Lemr, J. Soubusta, and M. Stobinska, *Phys. Rev. A* **89**, 062322 (2014).
- [24] K. Lemr, K. Bartkiewicz, A. Cernoch, J. Soubusta, and A. Miranowicz, *Phys. Rev. A* **85**, 050307 (2012).
- [25] A. S. Bracker, E. A. Stinaff, D. Gammon, M. E. Ware, J. G. Tischler, A. Shabaev, A. L. Efros, D. Park, D. Gershoni, V. L. Korenev, and I. A. Merkulov, *Phys. Rev. Lett.* **94**, 047402 (2005).
- [26] K. Bartkiewicz, A. Miranowicz, and S. K. Özdemir, *Phys. Rev. A* **80**, 032306 (2009).
- [27] P. van Loock, T. D. Ladd, K. Sanaka, F. Yamaguchi, K. Nemoto, W. J. Munro, and Y. Yamamoto, *Phys. Rev. Lett.* **96**, 240501 (2006).
- [28] B.-L. Fang, T. Wu, and L. Ye, *Quantum Inf. Comput.* **12**, 334 (2012).
- [29] B. L. Fang, T. Wu, and L. Ye, *Europhys. Lett.* **97**, 60002 (2012).
- [30] B. L. Fang, Q. M. Song, and L. Ye, *Phys. Rev. A* **83**, 042309 (2011).
- [31] J. I. Cirac, P. Zoller, H. J. Kimble, and H. Mabuchi, *Phys. Rev. Lett.* **78**, 3221 (1997).
- [32] S. Bose, P. L. Knight, M. B. Plenio, and V. Vedral, *Phys. Rev. Lett.* **83**, 5158 (1999).
- [33] L. M. Duan and H. J. Kimble, *Phys. Rev. Lett.* **90**, 253601 (2003).
- [34] D. E. Browne, M. B. Plenio, and S. F. Huelga, *Phys. Rev. Lett.* **91**, 067901 (2003).
- [35] Y. L. Lim, A. Beige, and L. C. Kwek, *Phys. Rev. Lett.* **95**, 030505 (2005).
- [36] S. D. Barrett and P. Kok, *Phys. Rev. A* **71**, 060310 (2005).
- [37] J. S. Xu, C. F. Li, L. Chen, X. B. Zou, and G. C. Guo, *Phys. Rev. A* **78**, 032322 (2008).
- [38] X. B. Zou, K. Li, and G. C. Guo, *Phys. Lett. A* **366**, 36 (2007).
- [39] X. B. Zou and W. Mathis, *Phys. Rev. A* **72**, 022306 (2005).
- [40] N. J. Cerf, *Phys. Rev. Lett.* **84**, 4497 (2000).
- [41] N. J. Cerf, *J. Mod. Opt.* **47**, 187 (2000).
- [42] I. Ghiu, *Phys. Rev. A* **67**, 012323 (2003).
- [43] H. Fan, K. Matsumoto, X. B. Wang, and M. Wadati, *Phys. Rev. A* **65**, 012304 (2001).
- [44] K. Bartkiewicz and A. Miranowicz, *Phys. Rev. A* **82**, 042330 (2010).
- [45] T. P. Spiller, K. Nemoto, S. L. Braunstein, W. J. Munro, P. van Loock, and G. J. Milburn, *New J. Phys.* **8**, 30 (2006).
- [46] S. E. Nigg, *Phys. Rev. A* **89**, 022340 (2014).
- [47] K. Nemoto and W. J. Munro, *Phys. Rev. Lett.* **93**, 250502 (2004).
- [48] P. van Loock, W. J. Munro, K. Nemoto, T. P. Spiller, T. D. Ladd, S. L. Braunstein, and G. J. Milburn, *Phys. Rev. A* **78**, 022303 (2008).
- [49] T. D. Ladd, P. van Loock, K. Nemoto, W. J. Munro, and Y. Yamamoto, *New J. Phys.* **8**, 184 (2006).
- [50] C. Bennett and G. Brassard, in *Proceedings of IEEE International Conference on Computers, Systems, and Signal Processing, Bangalore, India* (IEEE, New York, 1984), p. 175.
- [51] N. Gisin, G. E. Ribordy, W. Tittel, and H. Zbinden, *Rev. Mod. Phys.* **74**, 145 (2002).
- [52] H. Fan, H. Imai, K. Matsumoto, and X. B. Wang, *Phys. Rev. A* **67**, 022317 (2003).
- [53] H. Jeong, *Phys. Rev. A* **73**, 052320 (2006).
- [54] S. J. D. Phoenix, *Phys. Rev. A* **41**, 5132 (1990).
- [55] S. G. R. Louis, W. J. Munro, T. P. Spiller, and K. Nemoto, *Phys. Rev. A* **78**, 022326 (2008).
- [56] W. J. Munro, K. Nemoto, and T. P. Spiller, *New J. Phys.* **7**, 137 (2005).
- [57] S. J. van Enk and O. Hirota, *Phys. Rev. A* **64**, 022313 (2001).
- [58] P. van Loock, N. Lutkenhaus, W. J. Munro, and K. Nemoto, *Phys. Rev. A* **78**, 062319 (2008).